Comparison of a subrank to a full-rank time-reversal operator in a dynamic ocean

Geoffrey F. Edelmann,[a] Joseph F. Lingevitch, Charles F. Gaumond, David M. Fromm, and David C. Calvo
Acoustics Division, Naval Research Laboratory, 4555 Overlook Avenue SW, Washington, DC 20375-5320

(Received 30 March 2006; revised 8 August 2007; accepted 17 August 2007)

This paper investigates the application of time-reversal techniques to the detection and ensonification of a target of interest. The focusing method is based on a generalization of time-reversal operator techniques. A subrank time-reversal operator is derived and implemented using a discrete set of transmission beams to ensonify a region of interest. In a dynamic ocean simulation, target focusing using a subrank matrix is shown to be superior to using a full-rank matrix, specifically when the subrank matrix is captured in a period shorter than the coherence time of the modeled environment. Backscatter from the point target was propagated to a vertical 64-element source-receiver array and processed to form the sub-rank time-reversal operator matrix. The eigenvector corresponding to the strongest eigenvalue of the time-reversal operator was shown to focus energy on the target in simulation. Modeled results will be augmented by a limited at-sea experiment conducted on the New Jersey shelf in April–May 2004 measured low-frequency backscattered signal from an artificial target (echo repeater). [DOI: 10.1121/1.2783127]

PACS number(s): 43.60.Tj, 43.60.Fg, 43.30.Vh, 43.30.Re [DRD] Pages: 2706–2714

I. INTRODUCTION

The performance of active acoustic systems for target detection, tracking, and classification is degraded by: ocean variability, target motion, noise, and reverberation. One solution to the problems of noise and reverberation is time-reversal focusing. By focusing sound on the target, the target echo is increased, whereas reverberation from the surface and bottom is decreased; thus, increasing the signal-to-reverberation ratio.[1–3] Time reversal methods are still susceptible to ocean variability, particularly time-reversal operator methods for which the acquisition time of the data can exceed the coherence time of the medium. This paper will describe a subrank beam-based time-reversal operator technique that requires no environmental knowledge to find and focus sound on a target in a changing heterogeneous waveguide. The time-reversal operator is constructed with a few snapshots that are sufficient to capture the target, yet be measured within the period of temporal coherence. In addition to averaging over multiple snapshots, the target signal-to-noise-ratio was increased by utilizing a beam-based decomposition of the time-reversal operator (DORT) method.[1]

Time-reversal focusing of sound has been demonstrated in ultrasonic laboratory experiments[4,5] and at-sea experiments.[6–8] In these demonstrations, time-reversal techniques were applied to focus acoustic energy back to a probe source in a heterogeneous waveguide without requiring any knowledge of the propagation environment. The governing principle is the time-reversal invariance of the wave equation which implies that an outgoing wave will refocus to the original source location when the wavefront is reversed in time. In practice, a time-reversed wave is approximately realized using a time-reversal mirror (TRM) implemented by a source/receiver array (SRA) of collocated transducers. The TRM discretely samples a wavefront in space and time and retransmits a time-reversed version of the sampled signal.

Time-reversal mirrors have been used to detect and selectively focus acoustic energy on scatterers in a waveguide.[9,11] The DORT algorithm[11–13] considers a set of point scatterers. A response matrix is measured by sequentially transmitting impulses from individual source elements of the TRM and recording the backscattered echo from all targets on each receiver element. Ideally, the response matrix is symmetric and contains the measured Green's functions between the targets and every transducer of the TRM. In the DORT algorithm, this matrix is transformed into the frequency domain and factored by singular value decomposition. The resulting singular vectors approximate array weights associated with individual point targets. Retransmission of the conjugate array vectors yields a focus at the corresponding target location. This original theory has been expanded to include non-isotropic point scattering,[14] multiple scattering,[15] non-ideally separated targets,[13] scattering by extended objects,[16,17] and object imaging.[12,18]

In shallow water, the quality of the time-reversal focus is degraded by ocean change, target motion, SRA deformation, and noise.[6,19,20] In order to mitigate these effects, it is useful to formulate the DORT method in terms of a sum of covariance matrices over multiple snapshots of the gradually changing environment.[13] This formulation emphasizes the correspondence between time reversal and matched field processing (MFP) techniques which have been extensively developed in passive ocean acoustics.

In this paper, a subrank beam-based DORT technique for target detection in shallow water ocean environments is derived and demonstrated in simulation. The simulation is augmented with limited experimental data taken during the

[a]Electronic mail: geoffrey.edelmann@nrl.navy.mil

TREX-04 time-reversal focusing experiment. Sound propagation was modeled in a changing ocean waveguide as was measured between April and May 2004 on the New Jersey shelf. The drift of the echo repeater during the acquisition of the response matrix was the primary source of variability in time. Backscatter measurements of a drifting echo repeater acting as an artificial target were made with the Naval Research Laboratory's 64-channel SRA in the 500–600 Hz band. In Sec. II, the theory for the subrank beam-based time-reversal operator (TRO) is developed. In Sec. III, the theory is applied using a combination of numerical simulation and experimental data. It is shown that the subrank TRO is beneficial in cases where target drift or environmental fluctuations are significant during the time required to acquire the full-rank TRO.

II. THEORY

A. The time-reversal operator

The TRO

$$\mathbf{T} = \mathbf{K}^*\mathbf{K} \tag{1}$$

has been derived previously by Prada *et al.*[9] in the context of an acoustic iterative time-reversal process where $K_{ij}(\omega)$ is the frequency-domain transfer function between source element j and receive element i of a time-reversal mirror (complex conjugation is denoted by "an asterisk"). In this section, the basic theory relating the eigenvectors of the time-reversal operator to the one-way Green's functions (from individual targets to the TRM) is briefly summarized. Then, using the covariance matrix interpretation of the TRO (Sec. II C), we formulate a subrank time-reversal operator (Sec. II D).

The analysis of Prada treats the detection of a set of M isotropic point scatterers (targets) by an N element array ($M \leqslant N$) when multiple scattering between the targets can be neglected. Under these assumptions, the $\mathbf{K}$ matrix can be written in terms of the Green's function as,

$$\mathbf{K} = \mathbf{G}\boldsymbol{\Omega}\mathbf{G}^T A \tag{2}$$

where $G_{ij}(\omega)$ is a $N \times M$ matrix of normalized one-way Green's functions between source i and scatterer j, Ω_{ij} is a $M \times M$ diagonal matrix that includes the target scattering coefficients and spreading loss between the TRM and the targets, and $A(\omega)$ is the source function. Substituting Eq. (2) into Eq. (1) gives the TRO in terms of the one way Green's function as

$$\mathbf{T} = \mathbf{G}^*(\boldsymbol{\Omega}^*\mathbf{G}^H\mathbf{G}\boldsymbol{\Omega})\mathbf{G}^T|A|^2. \tag{3}$$

In order to relate the eigenvectors of $\mathbf{T}$ to the one-way Green's functions, we require that the TRM spans the water column with sufficient resolution to adequately sample the propagating modes, and that the targets are ideally separated (by more than a wavelength), so that the columns of $\mathbf{G}$ are approximately orthogonal,[6,9] that is

$$\mathbf{G}^H\mathbf{G} \approx \mathbf{I}, \tag{4}$$

where $\mathbf{I}$ is the identity matrix. In this case, the grouped term in Eq. (3) is a diagonal matrix and the TRO simplifies to

$$\mathbf{T} \approx \mathbf{G}^*|\boldsymbol{\Omega}|^2\mathbf{G}^T|A|^2 = \sum_{k=1}^{M} |\Omega_{kk}A|^2 G_{ik}^* G_{jk}. \tag{5}$$

From Eq. (5) and the orthogonality relationship, Eq. (4), we see that the nonzero eigenvalues of the TRO are $|\Omega_{kk}A|^2$ and the corresponding eigenvectors are given by the columns of $\mathbf{G}^*$. Thus, decomposition of the TRO yields the one way Green's functions from the time-reversal mirror to the scatterers.

B. Measurement of the time-reversal operator

The time-reversal operator can be obtained from a direct measurement of the response matrix, $\mathbf{K}$, on an N-element array using Eq. (1). This is the method used in previous ultrasonic tank experiments. In principle, $\mathbf{K}$ is a square symmetric matrix due to the reciprocity relationship between source and receiver locations.[21] In practice, the experimentally measured data matrix, $\mathbf{K}_d$, is acquired over a time interval involving multiple source transmissions; therefore, in applications where reciprocity is degraded over time by variability in the water column, source/receiver motion, and noise,[6,19,20] the direct measurement of the full response matrix becomes problematic. When considering these factors in the measurement of the $\mathbf{K}_d$ matrix, the question arises of how to construct a meaningful TRO in the case of low signal level and/or time varying conditions.

The main theoretical result of this paper is a generalized TRO derived below and given by

$$\mathbf{T}_d = \mathbf{K}_d^*\mathbf{K}_d^T, \tag{6}$$

where the T superscript denotes the transpose of the matrix. In this formulation, $\mathbf{T}_d$ is a Hermitian matrix regardless of the symmetry of $\mathbf{K}_d$. Additionally, it is not necessary that $\mathbf{K}_d$ be a square matrix. In the special case of a symmetric and square $\mathbf{K}_d$ matrix, Eq. (6) reduces to Eq. (1). We will show in Sec. II C that, for the case of a non-symmetric $\mathbf{K}_d$ matrix, Eq. (6) is interpreted as a sum over a set of covariance matrices.

C. The time-reversal operator and the covariance matrix

MFP is a common method for target detection and localization in the field of underwater acoustics. It is useful to frame the discussion of the time-reversal operator in the well developed terminology, known strengths, and limitations of MFP.[22] Most MFP techniques operate on a covariance matrix which is generally unknown and must be estimated. An ensemble of data snapshots (in time) are used to estimate the covariance matrix $\mathbf{C}$ as discussed in (Ref. 21, Chap. 10) and (Ref. 23, Chap. 15.4). These data contain signal and uncorrelated noise and are measured along an array of receivers. For an array with N hydrophones, $\mathbf{C}$ is a $N \times N$ matrix. In order to estimate $\mathbf{C}$, snapshots of recorded data are windowed, overlapped, and averaged with each other. If $\mathbf{k}_n$ is the nth snapshot of the complex pressure measured along the array at an angular frequency ω, then with L realizations we define the covariance matrix (suppressing the $1/L$ normalization constant) as

$$\mathbf{C} = \sum_{n=1}^{L} \mathbf{k}_n \mathbf{k}_n^H. \tag{7}$$

The covariance matrix $\mathbf{C}$ has L degrees of freedom and here we assume that the propagation environment has not changed appreciably during the period of data acquisition. Assuming that the noise and signal are uncorrelated, averaging a number of snapshots will improve the signal-to-noise ratio of the measurement. Additionally, as $\mathbf{C}$ is Hermitian, its eigenvalues are positive and its eigenvectors are orthogonal. With sufficient signal-to-noise ratio, the strongest eigenvalues correspond to any strong point scatterers or sources present in the data. The remaining eigenvalues represent noise. The conjugate of the first eigenvector of $\mathbf{C}$ is a steering vector that points in the direction of the strongest target. Transmitting this vector is equivalent to a single frequency version of time reversal and is a technique commonly referred to as eigenvector beamforming (Ref. 21, Chap. 10.3).

If the N measurements of $\mathbf{k}_n$ are made by transmitting a probe pulse from the N individual TRM transducers (or N orthonormal beams, Sec. II D), then the measured $\mathbf{k}_n$ vectors are the columns of the response matrix $\mathbf{K}$. If we have $L=N$ number of snapshots, then we can define an ensemble of the data snapshots as

$$\mathbf{K} = [\mathbf{k}_1, \mathbf{k}_2, \ldots, \mathbf{k}_N], \tag{8}$$

in which case the covariance matrix is equal to

$$\mathbf{C} = \mathbf{K}\mathbf{K}^H. \tag{9}$$

Equation (9) is simply the conjugate of the time-reversal operator as written in Eq. (6). Therefore, we define the TRO as

$$\mathbf{T} = \mathbf{K}^*\mathbf{K}^T = \mathbf{C}^*. \tag{10}$$

The TRO is the conjugate of the MFP covariance matrix.

D. Beam-space methods and the subrank time-reversal operator

The beam space time-reversal operator is a generalization of the element space TRO introduced by Prada.[9–11] In ocean experiments, measuring the backscatter from targets is hindered by ambient noise levels and small target scattering strengths. The generalization to beam space increases the total transmitted power by broadcasting from all transducers simultaneously instead of transmitting from individual transducer elements.

We formulate a beam representation of the response matrix by defining the amplitude and phase of the transducer elements on an array as the columns of a complex matrix $\mathbf{E}$. For an N-element array, N beams are chosen to satisfy the orthogonality condition $\mathbf{E}^H\mathbf{E}=\mathbf{E}\mathbf{E}^H=N\mathbf{I}$, where the superscript H denotes complex conjugate transpose and $\mathbf{I}$ is the identity operator. In this paper, we choose

$$E_{jk} = \exp(i2\pi j(k - N/2 - 1)/N), \tag{11}$$

where k is the index of the beam and j is the index of the transducer. With this phasing, beam index $k=N/2+1$ corresponds to a broadside transmission, beam indices $1 \leqslant k < N/2+1$ correspond to up-going plane waves, and indices $N/2+1 < k \leqslant N$ correspond to down-going plane waves. The beam-space representation is simply related to the element-space in terms of a discrete Fourier transform. Also, note that the incoming beams are given by the columns of $\mathbf{E}^*$ and they satisfy orthogonality, $\boldsymbol{E}^T\boldsymbol{E}^* = \boldsymbol{E}^*\boldsymbol{E}^T = N\boldsymbol{I}$ where the superscript T denotes transpose. The beam-space response matrix is related to the element-space matrix by the transformation,

$$\tilde{\mathbf{K}} = \mathbf{E}^T\mathbf{K}\mathbf{E}, \tag{12}$$

where the elements of $\tilde{K}_{jk}$ correspond to the response on the jth incoming beam due to an impulsive transmission on the kth outgoing beam. Note that $\tilde{\mathbf{K}}$ is symmetric if $\mathbf{K}$ is a symmetric matrix. The beam space TRO, $\tilde{\mathbf{T}}$, is defined by simply replacing $\mathbf{K}$ with $\tilde{\mathbf{K}}$ in Eq. (10) and interpreting the eigenvectors of this operator in a beam-space basis.

The original DORT theory was formulated in terms of a response matrix measured in the element-space basis. The beam-space basis, described above, is also a complete orthonormal set. We emphasize here that a complete, orthonormal basis is not a necessary requirement. In fact, backscatter from a single beam which ensonifies a target is sufficient to form the Green's function to that target. In many cases of interest, neither the target location nor the propagation characteristics of the beams will be known in advance. Therefore, it is advantageous to build the TRO from an ensemble of beams that will be more likely to successfully ensonify an arbitrarily located target. Compared to repeatedly transmitting the same beam (e.g., broadside) N times, transmitting a set of unique beams will illuminate different propagation paths between array and target. Additionally, each $\mathbf{k}_n$ records a different realization of the ambient noise field. However, due to the dynamic nature of the propagation medium in ocean acoustic applications, it may be impractical to measure the full matrix $\tilde{\mathbf{K}}$ in a sufficiently short period of time. In this case, a covariance matrix is formed using a subset of transmit beams. We refer to this as a subrank time-reversal operator.

The covariance matrix formulation of the TRO in Eq. (10) offers several advantages over the original theory. First, this convention forces the TRO to be a Hermitian matrix, even if the $\mathbf{K}_d$ matrix is no longer symmetric (changing medium) or $\mathbf{K}_d$ is deficient because not all of its elements were measured. Second, a subrank version of the $\mathbf{K}_d$ matrix can quickly characterize a target by transmitting only a subset of the possible beams $\mathbf{E}$, thereby mitigating the well-known "snapshot problem" in MFP literature by measuring the target before the medium changes.[22] Last, $\mathbf{K}_d$ can be overdetermined by measuring multiple realizations of a given transmit beam; this is especially useful if one beam is believed to be, through experience or simulation, superior at ensonfying the desired target (therefore $\mathbf{K}$ can be larger than $N \times M$). This paper will demonstrate that, in a dynamic environment, quickly measuring a coherent subset of beams can produce a superior TRO matrix than a TRO formed from a complete yet incoherent set of beams.

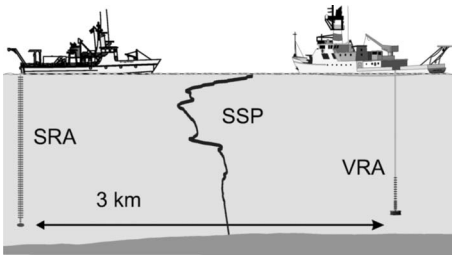

FIG. 1. The R/V Henlopen was moored in approximately 95-m deep water and is depicted with the source-receiver array (SRA) deployed from the A-frame. The array focused sound on the echo-repeater/probe source which was married beneath a short vertical receive array (VRA) deployed from the R/V ENDEAVOUR, which was slowly drifting away in 85-m deep water. A typical soundspeed profile (SSP) is shown.

III. SIMULATION AND EXPERIMENT

In this section, the main results of this paper are demonstrated numerically. Some supporting experimental measurements are also described. A time-reversal experiment (TREX-04) was conducted in April–May 2004 by the Naval Research Laboratory to test TRO methods for detection of an artificial target. The prevailing experimental conditions were utilized in the modeled environment. The ship geometry for the experiment is shown in Fig. 1.

A. Experimental setup

The following is a description of the equipment used and the environmental conditions present during TREX-04 from April 22 to May 4. The measured ocean conditions and experimental geometry were utilized for the simulation of acoustic propagation. Acoustic measurements were made in the region southwest of the Hudson Canyon off the coast of New Jersey. The water depth in this relatively flat region spanned from about 95 to 85 m over a range of approximately 3 km. The R/V HENLOPEN, moored in 95-m deep water, deployed a vertically suspended SRA. The 64-element SRA had 1.25 m interelement spacing for a total vertical aperture of 78.75 m. During the TREX-04 event described in this paper, the transmitted signals were 500–600 Hz LFM sweeps corresponding to a center frequency wavelength of about 2.7 m. The R/V ENDEAVOUR deployed a single Raytheon XF4 transducer below a 16-element, 8 m aperture dual nested vertical receive array (VRA). Although a longer aperture VLA would have been desirable, the short monitoring VLA does provide a glimpse at the spatial distribution of the acoustic field near the target. The XF4 was used both as a probe source and as an echo-repeater. When used as an echo-repeater, the VRA element closest to the XF4 (2 m separation) was echoed on the XF4. The R/V ENDEAVOUR drifted slowly away from the R/V HENLOPEN at approximately 0.6 km/h (0.3 knot) during acoustic transmissions. The echo repeater is considered to be the target in this paper. More details of TREX-04 are presented in Refs. 24–27.

Environmental measurements were made during this TREX-04 event as shown in Fig. 2. Twenty-one thermistor elements, which were physically coupled to the SRA, made continuous measurement of ocean temperature. Their record is shown in Fig. 2(a) over the two and a half days on interest. Conductivity, temperature, and depth (CTD) measurement were taken three times daily from the starboard winch. Overlapping temperature measurements recorded by the CTD casts and thermistor elements were in excellent agreement. The salinity profiles inferred from the ocean conductivity are shown in Fig. 2(b). Sound speed calculated from salinity and temperature appears in Fig. 2(c). From the point of view of measuring strong reverberation, the sound speed structure

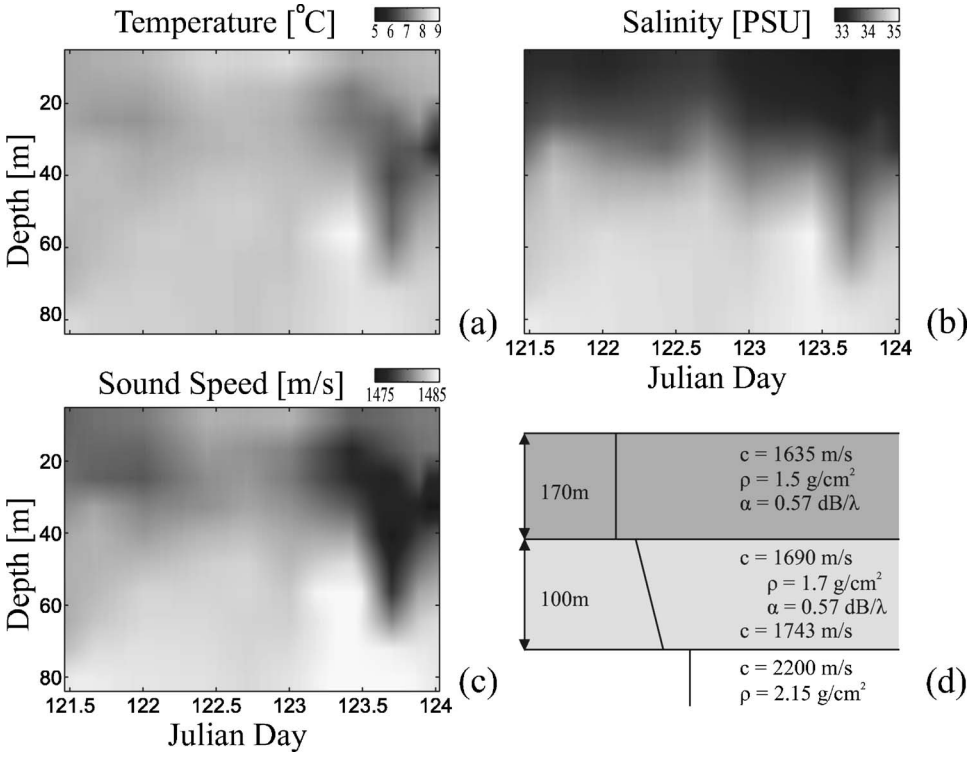

FIG. 2. (a) Twenty-one thermistors sampled the temperature field along the aperture of the SRA every 10 s. (b) Salinity measurements were inferred three times daily with CTD casts. (c) Calculated sound speed showing an upward refracting profile that traps energy in the water column. (d) The geoacoustic model for the experimental site area off the coast of New Jersey.

unfortunately created a sound channel that trapped acoustic energy in the water column thus preventing it from interacting with the bottom. The geoacoustic parameters in Fig. 2(d) are used for acoustic propagation modeling in this paper. These values are obtained from previous site surveys in the region.[26] The sediment layer has a sound speed that is greater than that of the water column. Measured reverberation was weak especially in light of the prevailing sound speed and relatively low acoustic transmission levels. Finally, the range-dependent bathymetry between the two ship positions was measured with an echo-sounder.

The coherence time of the channel was estimated to be at least 12 min. The point-to-point estimate was made by transmitting probe source pulses from the XF4 and cross-correlating the receptions at the 80-m depth SRA hydrophone in the half-hour prior to the TRO experiment. It includes environmental fluctuations as well as ship drift.

The data analyzed in this paper were measured during at a single event of the TREX-04 experiment conducted on May 1, 2004. Unfortunately, active acoustic transmissions were limited; therefore, this paper reinforces numerical simulations based upon the measured environment with acoustic data. These simulations are shown to agree with the available measured data and are also used to extrapolate when measured data were unavailable.

B. Time reversal of a probe source signal

This section will discuss at-sea measurements of time-reversal focusing and compare those measurements to simulations created by backpropagating the measured probe source signal data using computer models. By successfully simulating the measured time-reversal focus, we validate the use of both the propagation model and our detailed understanding of the environment. These simulations are then used to further elaborate on time-reversal operator methods.

On May 1st (Julian Day 122), a series of time-reversal foci were measured. The experimental setup of time-reversal focusing is shown in Fig. 1. The slowly drifting R/V ENDEVOUR deployed the XF4 probe source (PS) 2-m below the short VRA. The PS transmitted a Tukey windowed 1 s up-sweep chirp from 500 to 600 Hz. The PS chirp propagated about 2.8 km and was received on the SRA. The top element of the vertical SRA was suspended 3-m below the surface from the A-frame of the moored R/V HENLOPEN. The SRA digitally recorded, time-reversed, and retransmitted the PS transmission.[6] The time-reversed signal focused back at the original PS position. There was a 2 min turn around time from PS capture and time-reversal focus. Three of the foci measured on the VRA are shown in Fig. 3. Note that the VRA is 2-m above the original probe source position therefore the VRA is capturing only the upper half of the focal region. At these frequencies, the 3 dB down width of the focus was observed at 3 m as expected.[28]

The measured time-reversal foci are compared with simulated time-reversal foci created by backpropagating measured PS data using a computer model. In order to make accurate simulations of acoustic propagation, the *in situ* environment (bathymetry, thermistor temperature, salinity, and

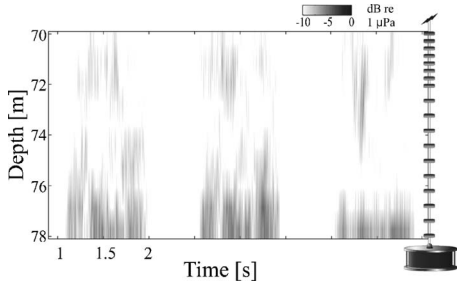

FIG. 3. A gray scale plot of three measured time-reversal foci are shown over depth and time. A diagram to the right of the time series shows the nested vertical-receiver array and its placement above the probe source. The probe source transmitted a Tukey windowed 1 s pulse which was measured on the source-receiver array about 2.8-km away. The signal was windowed, time-reversed, and retransmitted. The vertical-receiver array is measuring only the upper part of the focus.

GPS estimated ship locations) was used as described in Sec. III A. A wide-angle range-dependent parabolic equation model (RAM)[29] was used to simulate the broadband propagation. Time evolution of the water column and ship locations is incorporated into the simulations by using sound speed and ship location data that is 1 min older than the probe source reception. The environmental change includes temperature and salinity, but even more importantly incorporates slow range drifting of the PS. The R/V ENDEAVOUR was drifting away from the moored R/V HENLOPEN at approximately 0.6 km/h (0.3 knot). The drift was not fast enough to introduce Doppler spread into the PS signal.

Acoustic transmission loss simulated by backpropagating recorded PS data signals in the measured environment can be seen in Fig. 4. The upper left-hand panel shows the single-frequency (550 Hz) simulated backpropagation of a captured data PS ping in range and depth. The recorded PS ping used in this simulation was one of the three that were time-reversed, retransmitted, and focused on the VLA shown in Fig. 3. The time-reversal signal focuses at the same range as, and 2-m shallower than, the original PS position. Simulated backpropagation of a measured time-reversed PS signal is related to Bartlett matched-field processing.[22] Figure 4(c) shows the synthesised time series versus depth at the VRA that is simulated using the measured PS data from the SRA. These time-reversal foci simulations used the same PS signals recorded, time-reversed, and retransmitted to form the foci shown in Fig. 3. A side-by-side comparison of Figs. 3 and 4(c) shows that the backpropagated time series of the PS data are qualitatively identical to the measured time-reversal foci.

Next, MFP tracking of the PS position over time is used to verify that *in situ* ocean variability has been accurately modeled. Over the half-hour period of interest, the SRA recorded a PS signal almost every minute. Figures 4(b) and 4(d) depict a track of MFP results. A MFP ambiguity surface is made every minute over the course of half an hour. Range tracking at a fixed 80-m depth is displayed in Fig. 4(b). The most-likely range of the PS corresponds to the darkest peak. The global positioning system estimated range is overlaid as a black and white line. Using measured PS ping data, MFP is able to resolve accurately the PS in range. Note that no PS

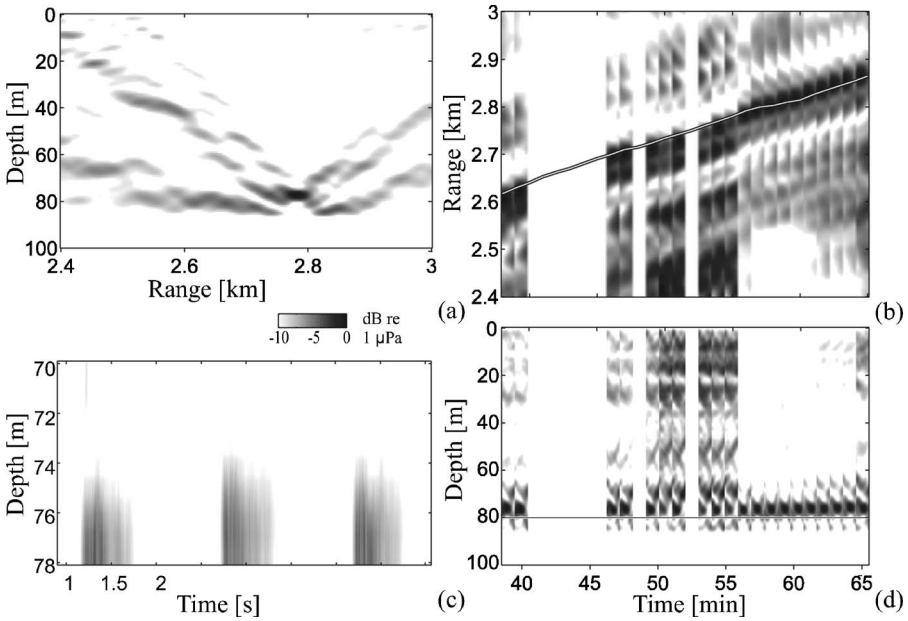

FIG. 4. Modeled backpropagation of probe-source signal data recorded on the SRA using the environmental measurements described in Fig. 1. (a) Single frequency ambiguity surfaces simulated at 550 Hz by backpropagating a measured probe-source data signal. The nominal range/depth of the probe-source is 2.8 km/80 m. (c) Coherent broadband simulation of the received time-reversal focus as it would be received on the VRA (three different realizations of the sweep are shown). (b) and (d) Tracking the target range and depth versus time. (b) Stacked plot of horizontal slices of the ambiguity surfaces at the nominal probe source depth. The solid line indicates the GPS estimated distance between the ships, one of which was freely drifting. (d) Vertical slices of the ambiguity surfaces at the nominal probe-source range. The solid line shows the measured depth of the probe source, which was different by 2 m.

signals were transmitted during the blank period (41–44 min). The MFP ambiguity surface of source depth over time appears in Fig. 4(d). Again, simulations reveal clear and successful MFP resolution over an extended period of time. Although accurate, the predicted PS depth is 2-m shallower than the depth sensor recordings (black and white line). This could be the result of a slight mismatch in bathymetric depth or the positioning of the depth sensor.

The correspondence between measured data and simulation demonstrates sufficiently an accurate understanding of the propagation environment between the two ships and a reliable method to simulate sound propagation during the TREX-04 experiment. These same simulation techniques will be used to verify and predict results in Sec. III C using time-reversal operator methods described Sec. II D.

C. Beam space methods and the time-reversal operator

This section will show simulations and limited results from a TRO target focusing portion of TREX-04. The degradation of TRO focusing due to environmental change and compensation via a subrank TRO measured over a shorter time frame shown. Additionally, the simulated TRO will be compared to the experimentally measured TRO and shown to be in excellent agreement.

We apply this approach to detecting targets in the ocean as follows: (1) a set of orthogonal transmit-beams is selected from Eq. (11) and the phase delays are applied to a 1.0 s LFM sweep (500–600 Hz) to form beams, (2) the transmit-beams are individually broadcast and 10 s of backscattered energy is recorded on all channels, (3) the backscattered signal is match filtered with the LFM and segmented in time to obtain the beam-element responses $k_{ij}(t)$ as a function of range from the array, (4) the beam-element responses are transformed to the frequency domain and singular vectors for the data TRO are formed, (5) the singular vector amplitude and phase delays are applied to the LFM sweep and the focusing pulse is transmitted from the SRA.

1. Simulated full-rank time-reversal operator focusing in a static ocean

In a static environment, measurement of the full TRO is desirable since this improves both the resolution of the focus and the signal-to-noise ratio. Ideal TRO focusing of a target at 80-m depth is displayed in Figs. 5(a) and 5(b). In this simulation, a complete set of 64 beams were transmitted and echoes from the target are recorded on the 64 element SRA. The TRO matrix was formed at the center frequency of the array (550 Hz) and decomposed into eigenvalues and eigenvectors. Only one strong eigenvalue was present, and the associated eigenvector corresponded to a weighting vector pointing acoustic energy back to the target. Ideal focusing of the first vector of the TRO is shown in Fig. 5(a). For the given geometry, attenuation, and frequency, this is the best focusing possible using TRO methods. A broadband signal can be sent using the eigenvector as an array weight. The incoherent average of the focus in Fig. 5(b), from 500 to 600 Hz, shows that an eigenvector made at the center frequency will successfully focus over the entire band. Applying the single frequency weight to a broadband signal smears the focus in range and depth but this can be an advantage if the target is mobile. In both Figs. 5(a) and 5(b) the energy is focused upon the target. The cylindrical spreading term has been removed from the transmission loss.

2. Simulated full-rank time-reversal operator focusing in a dynamic ocean

The ocean is a dynamic medium and environmental change can degrade TRO focusing. In this case, the simulated environment evolves as was recorded during the TRO portion of the TREX-04 experiment. Temperature, salinity, and, most importantly, ship-drift play a part in degrading the

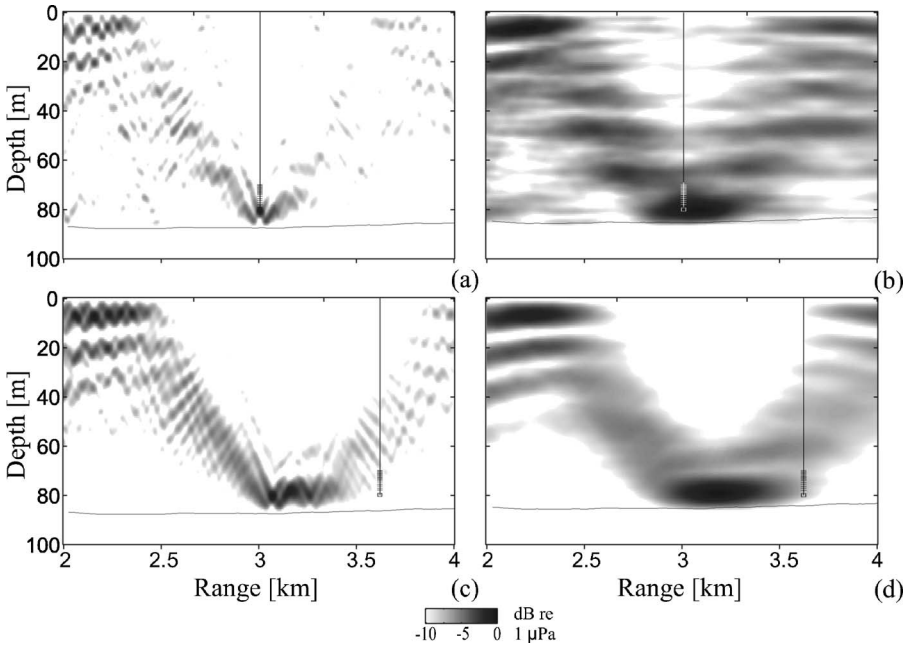

FIG. 5. Modeled TRO focusing simulation using 64 simulated beams. (a) Single frequency TRO focus of the first eigenvector in an inhomogeneous, range dependent, and static version of the typical ocean environment during the TREX-04 experiment and excluding ship drift. (b) Incoherent average of the broadband (500–600 Hz) TRO focus. (c) Single frequency TRO focus in a dynamically changing ocean including estimated ship drift. (d) Incoherent average of the dynamic broadband TRO focus. The black line represents the target collocated with the VRA which is drifting. Measuring all 64 beams, at one beam a minute, takes more than a hour which leads to a broadening of the focus. Note that the ship has drifted out of the center of the focal region.

TRO focus at the target position. The TRO is simulated by transmitting one beam per minute over the course of 64 min. The target was deployed from the R/V ENDEAVOUR which drifted almost 600 m over that time period in a changing ocean. Target focusing by weighting the SRA with the strongest eigenvector is shown in Fig. 5(c). The target has drifted beyond the focal position and is not successfully ensonified. Note how the focus is no longer sharp and has broadened in range and depth. The broadening is due to the averaging the Green's function over time and space and is the equivalent to the multiple constraint matching processor in MFP.[30] The broadband TRO method Fig. 5(d) peripherally ensonifies the target.

In a dynamic environment, one target can be associated with multiple eigenvalues. As the ocean changes the target back-scatter is incoherently distributed amongst multiple eigenvalues. In the static case, only one strong eigenvalue was present, the rest were associated with noise. In the dynamic case, the target has been spread over five eigenvalues. Practically speaking, unless there is concern about sending a coherent signal to the target (e.g., a communication signal), transmitting simultaneously multiple eigenvectors may prove advantageous. Transmission of the second TRO eigenvector [Fig. 6(a)] ensonifies the general target area and appears to be associated with the back-scatter simulated at later ranges. Transmitting both the first and second eigenvectors weighted by their respective eigenvalues appears in Fig. 6(b). Transmitting the first two eigenvectors has tightened the focus in range when compared to Fig. 5(c).

For the purpose of broadening the TRO focus and ensonifying the target, transmitting multiple eigenvectors did not prove advantageous during the environmental conditions present at the TREX-04 experiment.

3. Simulated subrank time-reversal operator focusing in a dynamic ocean

Measuring a subrank TRO can produce superior target ensonification in a dynamic ocean. During the TREX-04 experiment only a subset of the 64 beams were used to form the TRO; specifically, starting with the first beam, every 4th beam was transmitted ending on the 61st. These beams were

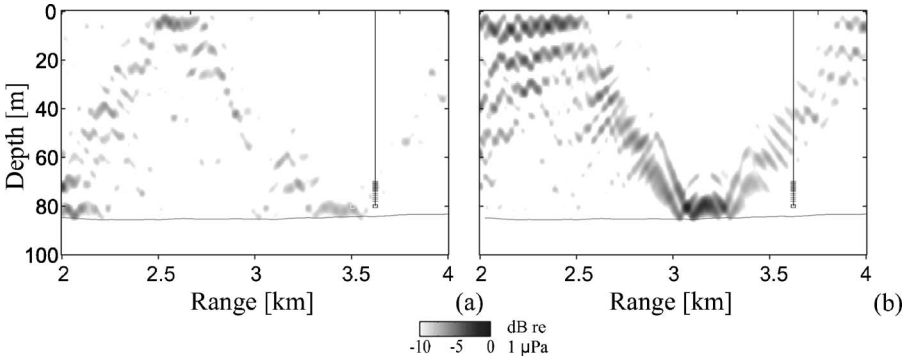

FIG. 6. Simulated single frequency TRO focusing using multiple eigenvectors in a dynamic ocean. (a) TRO focus using the second eigenvector and (b) TRO focusing using both the first and second eigenvectors weighted by their respective eigenvalues. No significant enhancement is seen. Over the 64 min used to measure the full-rank TRO the target has been spread into five significant incoherent eigenvalues (the other eigenvalues are noise). In the static environment [Figs. 5(a) and 5(b)], only one strong eigenvalue was present and corresponded to the target.

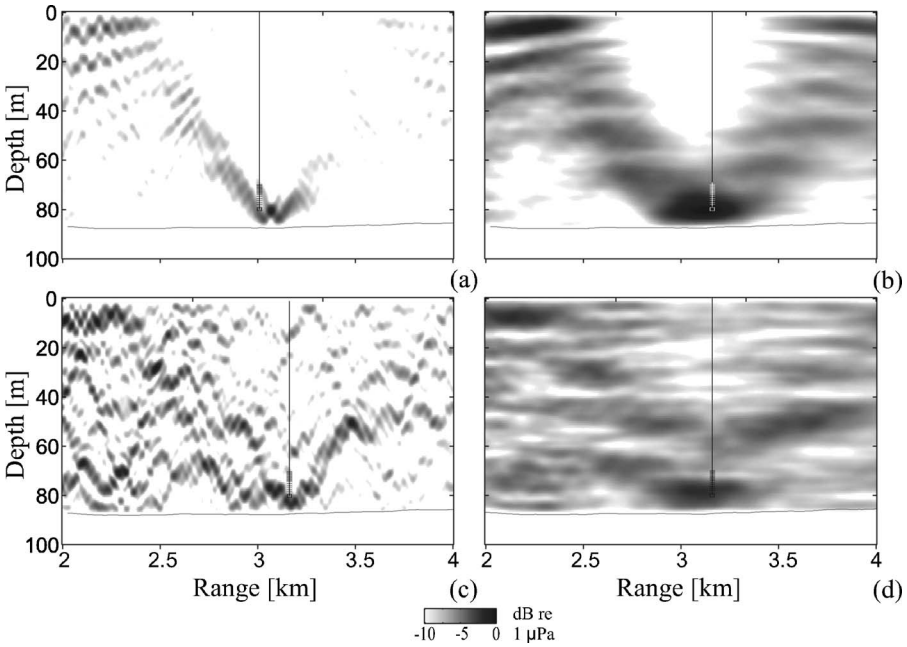

FIG. 7. Comparison of modeled backpropagation of simulated sub-rank TRO and measured subrank TRO. The subrank TRO was measured over a 15 min period using every fourth beam during the TREX-04 experiment. Backpropagation was modeled using a TRO constructed with simulated target response in (a) and (b) and from measured at-sea target response in (c) and (d). Subrank TRO focusing of simulated scatter: (a) Single frequency TRO focus of the first eigenvector in an inhomogeneous range-dependent and dynamic ocean with a drifting target. (b) Incoherent average of the broadband (500–600 Hz) TRO focus. Sub-rank TRO focusing of experimentally measured scatter: (c) Single frequency TRO focus of the first eigenvector. (d) Incoherent average of the broadband (500–600 Hz) TRO focus. In both cases, when the subrank TRO was estimated over a 15 min (instead of 64 min) period, the target was incoherently smeared into just two eigenvalues. In this dynamic case, the focus associated with the subrank TRO is superior to the focus of the full-rank TRO shown in Fig. 6.

not optimally selected; the only criterion was the desire to measure the TRO in a relatively short period of time (15 min). To ensure that the target was ensonified by at least a few beams, a broad range of launch angles were included. It should be noted that the steepest beams were absorbed by the sediment before reaching the target. Backscatter was present for only beams 21–41 in both the simulation and measurements made during TREX-04. Although it may have been optimal to select a narrower subset of beams between 21 and 41, such presumption would have required *a priori* estimates of acoustic propagation in the environment.

Backpropagation is modeled with a simulated subrank TRO matrix are shown in Fig. 7. Focusing of the first eigenvector at 550 Hz is shown in Fig. 7(a). The incoherent average of the broadband focus Fig. 7(b) ensonifies the desired target position. Before the first eigenvector was transmitted, 1 min is allowed to elapse in the simulated environment. Compared with the full rank matrix discussed in Sec. III C 2, the target focusing is significantly improved and is comparable to the TRO of the static ocean. The eigenvalue spread of the simulated TRO indicated that the target is only associated with two eigenvalues, with the majority of energy contained in the first value. Transmitting a subset of the beam matrix **E** greatly improved the simulated target focusing when that subset is measured within the coherence time of the channel.

4. Comparison of simulated to data derived subrank time-reversal operator focusing

In this section, the subrank TRO measured during the TREX-04 experiment is discussed and shown to focus on the desired target via propagation modeling. During the TREX-04 experiment a subset of 64 beams were transmitted and the back-scatter measured from an artificial target (echo repeater). As mentioned in Sec. III C 3, only beams 21–41 had sufficient signal level to trigger the echo repeater. The TRO was created using the measured back-scatter from all 15 beams. As no assumptions were made about which back-scatter events may or may not contain signal, the **K** matrix included ambient noise vectors.

Analysis of the measured TRO matrix is shown in Fig. 7. The single frequency backpropagation of the first TRO eigenvector is displayed in Fig. 7(c). The energy focuses in range and depth to almost the exact position as the purely simulated TRO in Fig. 7(a). The TRO target focusing appears more clearly in the broadband case, Fig. 7(d). Acoustic energy is incident upon the location of the drifting echo repeater.

Only two strong eigenvalues were present in the eigenvalue distribution of the measured TRO. The distribution is almost identical to the simulated TRO (not shown) with slightly more energy incoherently transferred into the second eigenvector. Surface, bottom, and volume scattering may have contributed to this slight decrease in target coherency. The coherence time of the channel was estimated to be approximately 12 min in the half-hour prior to the formation of the TRO matrix. The TRO matrix was created with 15 beams over 15 min, of which only 6 beams contributed to the signal. Thus, it is not surprising that the sub-rank TRO has little eigenvalue spread.

Comparing respectively Figs. 7(a) and 7(b) to Figs. 7(c) and 7(d) confirms that computer simulations are in agree-

ment with the measured data, and that acoustic energy was focused back on the drifting target during TREX-04. Additionally these results demonstrate that, in a dynamic medium, it is more important to measure a subrank TRO than a full-rank TRO because the target becomes incoherently distributed amongst multiple eigenvalues.

Focusing sound on the target not only increased the echo-repeater response, but also decreased the reverberation from the surface and bottom.[1–3] Figure 7(d) shows that the focal intensity at the target is about 7 dB higher than the surface (at the target range) and from the bottom (before and after target range). Thus, the self-generated reverberation that masks the target was greatly reduced.

IV. CONCLUSION

This paper describes a practical application of the TRO to target detection and ensonification. The TRO technique is based on the DORT algorithm and is capable of ensonifying a target while requiring neither a probe source, prior environmental knowledge, nor acoustic modeling predictions. The subrank TRO method was shown, in simulation, to focus acoustic energy back on an unknown drifting target. The modeled acoustic focus increased the target echo, while it simultaneously reduced reverberation from the surface and bottom; thereby, increasing detection, tracking, and classification capabilities.

The ocean is a time-dependent heterogeneous waveguide, where environmental fluctuations and target drift may be appreciable over the TRO acquisition window. Under these conditions, a target may be incoherently spread into multiple eigenvalues if a full-rank TRO matrix is measured. A simulated subrank TRO, acquired in a shorter time frame than the coherence time of the ocean, was shown to produce a superior focus. The subrank TRO is closely related to covariance matrix techniques of matched field processing.

ACKNOWLEDGMENTS

This work was supported by the Office of Naval Research. The authors would like to thank Richard Menis and Elisabeth Kim.

[1]J. F. Lingevitch, H. C. Song, and W. A. Kuperman, "Time reversed reverberation focusing in a waveguide," J. Acoust. Soc. Am. **111**, 2609–2614 (2002).
[2]H. C. Song, S. Kim, and W. A. Kuperman, "Environmentally adaptive reverberation nulling using a time reversal mirror," J. Acoust. Soc. Am. **116**, 762–768 (2004).
[3]S. Kim, W. A. Kuperman, W. S. Hodgkiss, H. C. Song, G. F. Edelmann, and T. Akal, "Echo-to-reverberation enhancement using a time reversal mirror," J. Acoust. Soc. Am. **115**, 1525–1531 (2004).
[4]M. Fink, "Time reversed acoustics," Phys. Today **50**, 34–40 (1997).
[5]M. Fink, "Time reversed acoustics" Sci. Am. (November 1999), 91–97 (1999).
[6]W. A. Kuperman, W. S. Hodgkiss, H. C. Song, T. Akal, C. Ferla, and D. Jackson, "Phase conjugation in the ocean: Experimental demonstration of an acoustic time-reversal mirror," J. Acoust. Soc. Am. **103**, 25–40 (1998).
[7]W. S. Hodgkiss, H. C. Song, W. A. Kuperman, T. Akal, C. Ferla, and D. Jackson, "A long range and variable focus phase-conjugation experiment in shallow water," J. Acoust. Soc. Am. **105**, 1597–1604 (1999).
[8]H. C. Song, W. A. Kuperman, and W. S. Hodgkiss, "A time-reversal mirror with variable range focusing," J. Acoust. Soc. Am. **103**, 3234–3240 (1998).
[9]C. Prada, J. L. Thomas, and M. Fink, "The iterative time reversal process: Analysis of the convergence," J. Acoust. Soc. Am. **103**, 3234–3240 (1998).
[10]E. Kerbrat, C. Prada, D. Cassereau, and M. Fink, "Ultrasonic nondestructive testing of scattering media using the decomposition of the time reversal operator," IEEE Trans. Ultrason. Ferroelectr. Freq. Control **49**(8), 1103–1113 (2002).
[11]C. Prada, S. Manneville, D. Spoliansky, and M. Fink, "Decomposition of the time reversal operator: Detection and selective focusing on two scatters," J. Acoust. Soc. Am. **99**, 2067–2076 (1996).
[12]N. Mordant, C. Prada, and M. Fink, "Highly resolved detection and selective focusing in a waveguide using D.O.R.T method," J. Acoust. Soc. Am. **105**, 2634–2642 (1999).
[13]C. Prada and J. L. Thomas, "Experimental subwavelength localization of scatterers by decomposition of the time reversal operator interpreted as a covariance matrix," J. Acoust. Soc. Am. **114**, 235–243 (2003).
[14]D. H. Chambers and A. K. Gautesen, "Time reversal for a single spherical scatterer," J. Acoust. Soc. Am. **109**, 2616–2624 (2001).
[15]A. J. Devaney, E. A. Marengo, and F. K. Gruber, "Time-reversal-based imaging and inverse scattering of multiply scattering point targets," J. Acoust. Soc. Am. **118**, 3129–3138 (2005).
[16]D. H. Chambers, "Analysis of the time-reversal operator for scatterers of finite size," J. Acoust. Soc. Am. **112**, 411–419 (2001).
[17]S. Hou, K. Solna, and H. Zhao, "Imaging of location and geometry for extended targets using the response matrix," J. Comput. Phys. **199**, 317–338 (2004).
[18]T. Folegot, C. Prada, and M. Fink, "Resolution enhancement and separation of reverberation from target echo with the time reversal operator decomposition," J. Acoust. Soc. Am. **113**, 3155–3160 (2003).
[19]K. G. Sabra, S. R. Khosla, and D. R. Dowling, "Broadband time-reversing array retrofocusing in noisy environments," J. Acoust. Soc. Am. **111**, 823–830 (2002).
[20]K. G. Sabra and D. R. Dowling, "Effects of time-reversing array deformation in an ocean wave guide," J. Acoust. Soc. Am. **115**, 2844–2847 (2004).
[21]F. B. Jensen, W. A. Kuperman, M. B. Porter, and H. Schmidt, *Computational Ocean Acoustics* (American Institute of Physics, New York, 1994).
[22]A. B. Baggeroer, W. A. Kuperman, and P. N. Mikhalevsky, "An overview of matched field methods in ocean acoustics," IEEE J. Ocean. Eng. **18**, 401–424 (1993).
[23]S. M. Kay, *Fundamentals of Statistical Signal Processing: Estimation Theory*, (Prentice–Hall, Upper Saddle River, N.J., 1993), Vol. **1**.
[24]D. M. Fromm, C. F. Gaumond, J. F. Lingevitch, R. Menis, D. C. Calvo, G. F. Edelmann, and E. Kim, "The effect of coherence and noise on the decomposition of the time reversal operator," OCEANS'05. MTS/IEEE TECHNO-OCEAN'05 (2005).
[25]C. F. Gaumond, D. M. Fromm, J. Lingevitch, R. Menis, G. Edelmann, D. Calvo, and E. Kim, "Application of DORT to active sonar," OCEANS'04. MTS/IEEE TECHNO-OCEAN'04, (2004), Vol. **4**, pp. 2230–2235.
[26]C. F. Gaumond, D. M. Fromm, J. F. Lingevitch, R. Menis, G. Edelmann, D. C. Calvo, and E. Kim, "Demonstration at sea of the decomposition-of-the-time-reversal-operator technique," J. Acoust. Soc. Am. **2**, 976–990 (2006).
[27]D. Calvo, C. F. Gaumond, D. M. Fromm, R. Menis, J. F. Lingevitch, G. F. Edelmann, and E. Kim, "Detection enhancement using multiple time-reversed guide sources in shallow water," OCEANS'05. MTS/IEEE TECHNO-OCEAN'05 (2005).
[28]S. Kim, G. F. Edelmann, W. A. Kuperman, W. S. Hodgkiss, H. C. Song, and T. Akal, "Spatial resolution of time-reversal arrays in shallow water," J. Acoust. Soc. Am. **110**, 820–829 (2001).
[29]M. D. Collins, "A split-step Padé solution for the parabolic equation method," J. Acoust. Soc. Am. **93**, 1736–1742 (1993).
[30]H. Schmidt, A. Baggeroer, and W. A. Kuperman, "Environmentally tolerant beamforming for high-resolution matched field processing: Deterministic mismatch," J. Acoust. Soc. Am. **88**, 1851–1862 (1990).